Pore Size Engineering and Mechanical Stability of the Cubic Mesoporous Molecular Sieve SBA-1

A. Vinu,[†,‡] V. Murugesan,[‡] and Martin Hartmann*[,†]

Department of Chemistry, Chemical Technology, University of Kaiserslautern, P.O. Box 3049, D-67653 Kaiserslautern, Germany, and Department of Chemistry, Anna University, Chennai 600025, India

Received November 12, 2002

The influence of HCl/surfactant ratio (n_{HCl}/n_S) and synthesis time on the synthesis of the cubic mesoporous molecular sieve SBA-1 were investigated to obtain high-quality materials. The samples prepared at a n_{HCl}/n_S ratio of 280 were found to exhibit a higher degree of structural ordering, a higher specific surface area, and a higher specific pore volume as compared to materials prepared at a lower n_{HCl}/n_S ratio. The pore diameter of SBA-1 can be tuned from 2.3 to 3.0 nm by simply adjusting the synthesis time between 1 and 72 h. The pore volume increases from 0.7 to 1.03 cm^3/g with a concomitant decrease of the surface area from 1430 to 1100 m^2/g. Moreover, the stability of the materials toward washing with water was improved by increasing the crystallization time from 1 to 72 h. The mechanical stability of SBA-1 was also investigated using *n*-heptane and cyclohexane adsorption in addition to nitrogen adsorption. The mechanical stability of SBA-1 is high; by compression of about 217 MPa, the specific pore volume calculated from nitrogen adsorption decreases by 19.7%, whereas the pore volume calculated from the *n*-heptane and cyclohexane adsorption decreases by 12.5% and 7.5%, respectively. These results together with the large difference between the pore volumes obtained by nitrogen and organics adsorption indicate that the presence of microporosity in the SBA-1 pore walls has to be considered. SBA-1 is mechanically more stable as compared with hexagonal mesoporous materials such as MCM-41 and SBA-15, but exhibits similar mechanical stability as compared to the cubic MCM-48 material.

Introduction

Mesoporous molecular sieves have attracted considerable attention in recent years since the discovery of the M41S family of mesoporous materials by researchers of the Mobil Oil Corporation.[1] Originally, this family has been classified into three subgroups: a hexagonal (MCM-41), a cubic (MCM-48), and a lamellar phase (MCM-50). Among these novel materials, phases with a three-dimensional pore system are believed to be more advantageous for catalytic applications than phases having a one-dimensional array of pores. It is surmised that three-dimensional pore arrangements are more resistant to pore locking and allow faster diffusion of reactants. Surprisingly, the majority of studies published so for deal with phases having a one-dimensional pore system, viz. MCM-41 and SBA-15. Huo et al.[3−6] have synthesized a novel mesoporous molecular sieve with a three-dimensional cubic structure (space group $Pm\bar{3}n$) of uniform pore size. The novel material, denoted SBA-1, has a cage-type structure with open windows[7] and was formed by a (S^+ X^- I^+) pathway (cationic surfactants (S^+), halogen anions (X^-), and cationic silicic acid species (I^+)). Tatsumi and co-workers have investigated the synthesis of V- and Mo-containing SBA-1[8] and gained control of the crystal morphology.[9] More recently, we reported the direct synthesis of AlSBA-1 containing exclusively tetrahedrally coordinated aluminum and the catalytic activity of this material in the isomerization of *n*-decane,[10] as well as the synthesis of cobalt-containing SBA-1.[11]

Materials with uniform and tunable pore sizes are expected to play an important role in a number of applications that range from catalysis, to molecular separations and sorption of very bulky molecules,[12] and

* To whom correspondence should be addressed. Phone: +49-631-205-3559. Fax: +49-631-205-4193. E-mail: hartmann@rhrk.uni-kl.de.
† University of Kaiserslautern.
‡ Anna University.

(1) Kresge, C. T.; Leonowicz, M. E.; Roth, W. J.; Vartuli, J. C.; Beck, J. S. *Nature* **1992**, *359*, 710.
(2) Luan, Z.; Xu, J.; Kevan, L. *Chem. Mater.* **1998**, *10*, 3699.
(3) Huo, Q.; Margolese, D. I.; Ciesla, U.; Feng, P.; Gier, T. E.; Sieger, P.; Leon, R.; Petroff, P. M.; Schüth, F.; Stucky, G. D. *Nature* **1994**, *368*, 317.
(4) Huo, Q.; Margolese, D. I.; Ciesla, U.; Demuth, D. G.; Feng, P.; Gier, T. E.; Sieger, P.; Firouzi, A.; Chmelka, B. F.; Schüth, F.; Stucky, G. D. *Chem. Mater.* **1994**, *6*, 1176.
(5) Huo, Q.; Leon, R.; Petroff, P. M.; Stucky, G. D. *Science* **1995**, *268*, 1324.
(6) Huo, Q.; Margolese, D. I.; Stucky, G. D. *Chem. Mater.* **1996**, *8*, 1147.
(7) Sakamoto, Y.; Kaneda, M.; Terasaki, O.; Zhao, D.; Kim, J. M.; Stucky, G.; Shin, H. J.; Ryoo, R. *Nature* **2000**, *408*, 449.
(8) (a) Dai, L.-X.; Tabata, K.; Suzuki, E.; Tatsumi, T. *Chem. Mater.* **2001**, *13*, 208. (b) Dai, L.-X.; Teng, Y.-H.; Tabata, K.; Suzuki, E.; Tatsumi, T. *Chem. Lett.* **2000**, 794.
(9) Che, S.; Sakamoto, Y.; Terasaki, O.; Tatsumi, T. *Chem. Mater.* **2001**, *13*, 2237.
(10) Vinu, A.; Dedecek, J.; Murugesan, V.; Hartmann, M. C*hem. Mater.* **2002**, *14*, 2433.
(11) Hartmann, M.; Vinu, A.; Elangovan, S. P.; Murugesan, V.; Böhlmann, W. *Chem. Commun.* **2002**, *11*, 1238.
(12) Corma, A.; Navarro, M. T.; Perez-Pariente, J. *J. Chem. Soc., Chem. Commun.* **1994**, 147.

10.1021/cm0213523 CCC: $25.00
Published on Web 03/01/2003

to the fabrication of semiconductors, semiconductor nanowires, and low dielectric devices.[13,14] Kim and Ryoo[15] tried to increase the pore diameter of SBA-1 by using surfactants with different tail lengths or by expanding the micelles with trimethylbenzene as a swelling agent. This method of mesopore size control is, however, limited and results in a decrease of structural order with increasing pore diameter, probably due to mismatches in the surfactants head-to-tail packing ratio. It is also obvious that the introduction of large amounts of swelling agents during the synthesis is not an optimal procedure for an industrial-scale synthesis since additional processes for separation and recycling of the swelling agent are needed. It is, therefore, desirable to increase the pore size of the mesoporous materials without the addition of swelling agents.

Although the adsorption of nitrogen[1,16−19] and water[16,20−22] has been thoroughly investigated over mesoporous molecular sieves, adsorption of organics over these materials has only been scarcely addressed. Few studies have dealt with the adsorption of hydrocarbons such as benzene,[23−25] toluene,[25] cyclopentane,[26,27] cyclohexane,[22,26−29] propane,[30] and methane[31] on MCM-41. Rathousky et al.[26] and Franke et al.[27] have studied the influence of temperature on the adsorption of cyclohexane on MCM-41. Beck et al.[32] and Nguyen et al.[23] reported benzene adsorption isotherms on a series of MCM-41 and AlMCM-41 samples, which were prepared by using surfactants with various carbon chain lengths. Recently, we have studied the adsorption of benzene, cyclohexane, and *n*-heptane for assessing the mechanical stability of MCM-48 and SBA-15 molecular sieves.[33−35]

The performance of mesoporous silicas in adsorption and catalysis is influenced by their pore volume and pore size, which controls the adsorption capacity and allows fast diffusion of reactants and products. Pore volume, pore diameter, and surface area are controlled by synthesis, but calcination is needed to allow access to the porosity and a shaping procedure is often needed to prepare catalyst pellets. Therefore, mechanical stability is an important characteristic with respect to industrial applications where the powders typically obtained by hydothermal synthesis are subject to a shaping process. Few studies on the mechanical stability of mesoporous molecular sieves, viz. MCM-41, MCM-48, and SBA-15 have been reported.[33−43] Gusev et al. showed that mesoporous materials such as MCM-41 are considerably less mechanically stable as compared to zeolites, alumina, mica, illite, kaolin, halloysite, and silica gels.[36] It has also been reported that the hexagonal mesoporous material FSM-16 loses structural order upon compression.[41]

In the present contribution, we report a new strategy to engineer the pore size of the cubic mesoporous molecular sieve SBA-1 during the synthesis by simply adjusting the crystallization time without addition of any organic swelling agents. Furthermore, we show that the structural order of SBA-1 can be improved by adjusting the hydrochloric acid-to-surfactant ratio. Moreover, the mechanical stability of cubic SBA-1 materials was studied by applying different pelletizing pressures and subsequent characterization by XRD and N_2 adsorption. Cyclohexane and *n*-heptane adsorption isotherms were recorded to evaluate the uptake of organics of the compressed materials. It has been found that SBA-1 has a comparable stability to MCM-48, which also possesses a three-dimensional array of mesopores.

Experimental Section

Surfactant Preparation. The surfactant cetyltriethylammonium bromide (CTEABr) was synthesized by reaction of 1-bromohexadecane with an equimolar amount of triethylamine in ethanolic solution under reflux for 2 days. The resultant surfactant CTEABr was purified by recrystallization from a chloroform/ethyl acetate mixture.

Synthesis of SBA-1. SBA-1 was prepared under acidic conditions using CTEABr as the surfactant and tetraethyl orthosilicate (TEOS) as the silica source. A typical synthesis procedure was as follows: Solution A was prepared by adding 0.81 g of CTEABr to the required amount of an aqueous HCl solution and stirred for 30 min to obtain a homogeneous solution. TEOS was precooled to 0 °C and then added to

(13) Tanev, P. T.; Pinnavaia, T. *Chem. Mater.* **1996**, *8*, 2068.
(14) Brunisma, P. J.; Hess, N. J.; Bontha, J. R.; Liu, J.; Baskaran, S. *Mater. Res. Soc. Proc.* **1997**, *359*, 710.
(15) Kim, M. J.; Ryoo, R. *Chem. Mater.* **1999**, *11*, 487.
(16) Branton, P. J.; Hall, P. G.; Sing, K. S. W.; Reichert, H.; Schüth, F.; Unger, K. K. *J. Chem. Soc., Faraday Trans.* **1994**, *90*, 2965.
(17) Llewellyn, P. L.; Grillet, Y.; Schüth, F.; Reichert, H.; Unger, K. K. *Microporous Mater.* **1994**, *3*, 345.
(18) Kruk, M.; Jaroniec, M.; Sayari, A. *J. Phys. Chem. B.* **1997**, *101*, 583.
(19) Ravikovitch, P. I.; Wie, D.; Chuch, W. T.; Haller, G. L.; Neimark, A. V. *J. Phys. Chem. B* **1997**, *101*, 3671.
(20) Llewellyn, P. L.; Schüth, F.; Grillet, Y.; Rouquerol, F.; Rouquerol, J.; Unger, K. K. *Langmuir* **1995**, *11*, 574.
(21) Cauvel, A.; Brunel, D.; Di Renzo, F.; Garrone, E.; Fubini, B. *Langmuir* **1997**, *13*, 2773.
(22) Chen, C.-Y.; Li, H.-X.; Davis, M. E. *Microporous Mater.* **1993**, *2*, 17.
(23) Nguyen, C.; Sonwane, C. G.; Bhatia, S. K.; Do, D. D. *Langmuir* **1998**, *14*, 4950.
(24) Jänichen, J.; Stach, H.; Busio, M.; Van Wolput, J. H. M. C. *Thermochim. Acta* **1998**, *312*, 33.
(25) Boger, T.; Roesky, R.; Glaeser, R.; Ernst, S.; Eigenberger, G.; Weitkamp, J. *Microporous Mater.* **1997**, *8*, 79.
(26) Rathousky, J.; Zukal, A.; Franke, O.; Schulz-Ekloff, G. *J. Chem. Soc., Faraday Trans.* **1995**, *91*, 937.
(27) Franke, O.; Schulz-Ekloff, G. J.; Rathousky, J.; Starech, J.; Zukal, A. *J. Chem. Soc., Chem. Commun.* **1993**, 724.
(28) Chen, C.-Y.; Xiao, Si.-Q.; Davis, M. E. *Microporous Mater.* **1995**, *4*, 1.
(29) Gläser, R.; Roesky, R.; Boger, T.; Ernst, S.; Eigenberger, G.; Weitkamp, J. *Stud. Surf. Sci. Catal.* **1997**, *105A*, 695.
(30) Maddox, M. W.; Sowers, S. L.; Gubbins, K. E. A*dsorption* **1996**, *2*, 23.
(31) Loneva, M. A.; Newman, G. K.; Harwell, J. H. *AIChE Symp. Ser.* **1995**, *3033.9*, 40.
(32) Beck, J. S.; Vartuli, J. C.; Roth, W. J.; Leonowicz, M. E.; Kresge, C. T.; Schmitt, K. D.; Chu, C. T. W.; Olson, D. H.; Sheppard, E. W.; McCullan, S. B.; Higgins, J. B.; Schlenker, J. L. *J. Am. Chem. Soc.* **1992**, *114*, 10834.
(33) Hartmann, M.; Bischof, C. *J. Phys. Chem. B* **1999**, *103*, 6230.
(34) Hartmann, M.; Bischof, C. *Prepr.—Am. Chem. Soc., Div. Pet. Chem.* **2001**, *46*, 23.
(35) Hartmann, M.; Vinu, A. *Langmuir* **2002**, *18*, 8010.
(36) Gusev, V. Y.; Feng, X.; Bu, Z.; Haller, G. L.; O'Brien, J. A. *J. Phys. Chem. B* **1996**, *100*, 1985.
(37) Koyano, K. A.; Tatsumi, T. *J. Phys. Chem. B* **1997**, *101*, 9436.
(38) Tatsumi, T.; Koyano, K. A.; Tanaka, Y.; Nakata, S. *Chem. Lett.* **1997**, 469.
(39) Tatsumi, T.; Koyano, K. A.; Tanaka, Y.; Nakata, S. *J. Porous Mater.* **1999**, *6*, 13.
(40) Desplantier-Giscard, D.; Collart, O.; Galarneau, A.; Van der Voort, P.; Di Renzo, F.; Fajula, F. *Stud. Surf. Sci. Catal.* **2000**, *129*, 665.
(41) Ishikawa, T.; Matsuda, M.; Vasukawa, A.; Kandori, K.; Inagaki, S.; Fukushima, T.; Konda, S. *J. Chem. Soc., Faraday Trans.* **1996**, *92*, 1985
(42) Springuel-Huet, M.-A.; Bonardet, J.-L.; Gédéon, A.; Yue, Y.; Rommannikov, V. N.; Fraissard, J. *Microporous Mesoporous Mater.* **2001**, *44−45*, 775.
(43) Galarneau, A.; Desplantier-Giscard, D.; Di Renzo, F.; Fajula, F. *Catal. Today* **2001**, *68*, 191.

solution A (also cooled to 0 °C) under vigorous stirring. Stirring was continued for another 5 h at 0 °C. Thereafter, the synthesis gel was heated to 100 °C. A first set of samples was prepared by keeping the gel at different crystallization times between 1 and 72 h. The "parent" material, which was heated at 100 °C for only 1 h, is denoted as SBA-1C. The other samples are designated as SBA-1-(*x*H) and SBA-1-(*y*HW), where *x*H indicates the synthesis time in hours (before washing with water) and *y*HW specifies the synthesis time of those samples, which were washed with water after synthesis. A second set of samples was prepared by changing the molar hydrochloric acid-to-surfactant ratio and was denoted as SBA-1-(*z*S) where *z* denotes the molar hydrochloric acid-to-surfactant ratio. The resultant solid products were filtered (with and without washing with water) and dried in air at 100 °C overnight. The molar composition of the gel was 1:0.2:10−56:125−700 TEOS:CTEABr:HCl:H_2O. The as-synthesized materials were then calcined under nitrogen by raising the temperature from 20 to 550 °C in 8 h and keeping it at 550 °C for another 10 h in air.

Characterization. The powder X-ray diffraction patterns of SBA-1 materials were collected on a Siemens-axs D5005 diffractometer using Cu Kα (λ = 0.154 nm) radiation. The diffractograms were recorded in the 2θ range of 0.8−10° with a 2θ step size of 0.01° and a step time of 10 s. High-resolution thermogravimetry analysis (SETARAM setsys 16MS) was carried out under a nitrogen atmosphere in the temperature range from 20 to 500 °C with a heating rate of 5 K/min. The sample was kept for an hour at 500 °C and subsequently heated to 600 °C in air with a heating rate of 5 K/min. Nitrogen adsorption and desorption isotherms were measured at 77 K on a Quantachrome Autosorb 1 sorption analyzer. All samples were outgassed for 3 h at 250 °C under vacuum ($p < 10^{-5}$ hPa) in the degas port of the adsorption analyzer. The specific surface area was calculated using the BET model. The pore size distributions were obtained from the adsorption and desorption branch of the nitrogen isotherms using the corrected form of the Kelvin equation by means of the Barrett−Joyner−Halenda method as proposed by Kruk et al.:[44]

$$r(p/p_0) = 2\gamma_L/RT \ln[p_0/p] + t(p/p_0) + 0.3 \text{ nm} \qquad (1)$$

In eq 1, V_L is the molar volume of the liquid adsorbate, γ is its surface tension (8.88×10^{-3} N/m), R is the gas constant (8.314 J/(mol·K)), and T is the absolute temperature (77 K). $t(p/p_0)$ is the statistical film thickness of nitrogen adsorbate in pores of the SBA-1 as a function of the relative pressure p/p_0). The diameter of the SBA-1 cavity is calculated using eq 2, which was recently proposed by Ravikovitch and Neimark:[45]

$$D_{me} = a(6\epsilon_{me}/\pi\nu)^{1/3} \qquad (2)$$

In eq 2, D_{me} is the diameter of the cavity of a cubic unit cell of length a, ϵ_{me} is the volume fraction of a regular cavity, and ν is the number of cavities present in the unit cell (for $Pm\bar{3}n$ space group, $\nu = 8$).

To test the mechanical stability of cubic SBA-1 materials, the calcined samples were compressed in a steel die of 24-mm diameter, using a hand-operated press, for 30 min. The four different external pressures applied (0, 43, 108, and 217 MPa) were calculated from the external force applied and the diameter of the die. Subsequently, the obtained disk was crushed and sieved to obtain pellets with a diameter of 0.2−0.35 nm, which were used for all further measurements. The unpressed material was denoted as SBA-1C. The other samples were denoted as SBA-1(*P*), where *P* specifies the pressure in MPa. Cyclohexane adsorption at 298 K and *n*-heptane adsorption isotherms at different temperatures (286, 298, and 313 K) were recorded using a home-built volumetric adsorption apparatus. Prior to the adsorption experiments, the samples were dehydrated at 200 °C under vacuum ($p < 10^{-6}$ hPa) for 4 h.

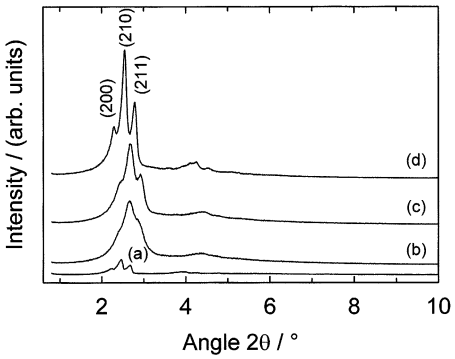

Figure 1. XRD powder patterns of SBA-1 materials prepared at different n_{HCl}/n_S ratios: (a) as-synthesized SBA-1; (b) SBA-1-(50S); (c) SBA-1-(140S); (d) SBA-1-(280S).

Table 1. Structural Parameters of SBA-1 Samples Prepared at Different n_{HCl}/n_S Ratios.

sample	n_{HCl}/n_S	a_0 (nm)	A_{BET} (m^2/g)	pore volume (cm^3/g)	pore diameter $d_{p,ads}$ (nm)
SBA-1-(280S)	280	77.7	1427	0.71	2.3
SBA-1-(140S)	140	73.8	1297	0.69	2.2
SBA-1-(50S)	50	74.1	1151	0.60	2.2

Results and Discussion

Variation of the Hydrochloric Acid-to-Surfactant Ratio (n_{HCl}/n_S). Figure 1 shows the X-ray powder diffraction patterns of a typical pure-silica SBA-1 sample before (a) and after calcination (b). For both the as-synthesized and the calcined sample, three reflections in the region 2θ = 2−3.5° are observed which are indexed to the (200), ($\bar{2}$10), and (211) reflections of the cubic space group $Pm\bar{3}n$. Higher order reflections are observed in the region 2θ = 3.5−6.5°, which are a superposition of various reflections which can be indexed according to the $Pm\bar{3}n$ space group. The length of the cubic cell a_0 is calculated using the formula $a_0 = d_{210}\sqrt{5}$ (Table 1). The observed d spacings are compatible with the cubic $Pm\bar{3}n$ space group. After calcination, the intensity of the XRD reflections is substantially larger compared to those measured for the as-synthesized sample.

The XRD patterns of samples prepared using different molar hydrochloric acid (HCl) to surfactant (S) ratios n_{HCl}/n_S are also shown in Figure 1. It can be seen that the interplanar spacing increases with increasing n_{HCl}/n_S ratio. An intense peak representing the (210) reflection is clearly observed for all samples, but intense and sharp (200) and (211) reflections are only observed for the SBA-1-(280S) sample. The observed increase in peak width is probably a consequence of the decrease in scattering domain size, or more likely of the growing disorder with decreasing n_{HCl}/n_S ratio. While the sample prepared using a n_{HCl}/n_S ratio of 280 (SBA-1-(280S)) exhibits a well-ordered cubic SBA-1 structure, the structural order decreases from cubic to less ordered cubic with decreasing n_{HCl}/n_S ratio (Figure 1).

Information on the textural properties of porous solids are typically obtained from low-temperature nitrogen adsorption isotherms, which allow calculation of the specific surface area, specific pore volume, and mesopore

(44) Kruk, M.; Jaroniec, M.; Sayari, A. *Langmuir* **1997**, *13*, 6267.
(45) Ravikovitch, P. I.; Neimark, A. V. *Langmuir* **2002**, *18*, 1550.

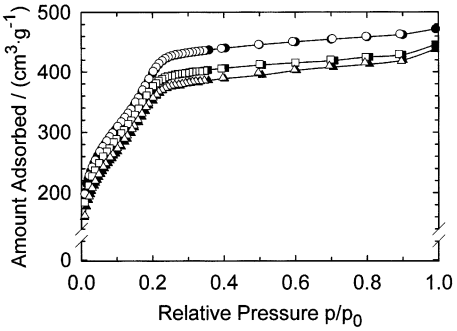

Figure 2. Nitrogen adsorption isotherms (adsorption, closed symbols; desorption, open symbols) of SBA-1 materials prepared at different n_{HCl}/n_S ratios: (●) SBA-1-(280S); (■) SBA-1-(140S); (▲) SBA-1-(50S).

size distribution. The nitrogen adsorption−desorption isotherms and structural parameters of the SBA-1 samples are displayed in Figure 2 and Table 1, respectively. As shown in Figure 2, the isotherm for calcined SBA-1C is of type IV according to the IUPAC classification, characteristic of mesoporous materials with a narrow pore size distribution. However, the capillary condensation step is relatively broad ($p/p_0 = 0.15-0.25$) as compared to that of MCM-41 or MCM-48 despite the high periodicity of the SBA-1 structure as evident from the corresponding XRD pattern. This result has been ascribed to the peculiarity of the SBA-1 structure consisting of two types of cagelike pores.[7] Moreover, the theoretical basis for the BJH analysis becomes fairly weak for those systems, where the capillary condensation step is at $p/p_0 = 0.15$, which is below the stabilization limit of the meniscus ($p/p_0 = 0.42$). Furthermore, on the basis of the assumption of cylindrical pore geometry, the BJH model is not well-suited to draw a definite conclusion about the pore size in SBA-1 with its three-dimensional cubic, cage-like type structure.[7] However, despite the assumption of two types of pores in SBA-1,[46] typically only one peak is observed in the BJH pore size distribution analysis. It has been suggested that the two peaks have coalesced because the ratio of the two pore size diameters is estimated to be ca. 1.1.[7]

The form of the isotherm is similar for all samples under investigation, but the amount of nitrogen adsorbed decreases with decreasing n_{HCl}/n_S ratio. The mesopore filling step in the isotherms of the samples which were prepared with a reduced n_{HCl}/n_S ratio is comparatively less well-developed probably due to a lower extent of long-range ordering. The specific surface area amounts to 1450 m^2/g for SBA-1-(280S) and decreases to 1150 m^2/g for SBA-1-(50S), whereas the specific pore volume decreases from 0.71 to 0.60 cm^3/g for the same samples. The pore diameters calculated using the modified BJH model (eq 1) do not vary with HCl content of the gel (cf. Table 1), whereas the pore size distribution is broadened with decreasing HCl concentration (not shown). The observed reduction in surface area, pore volume, and the observed broadening of pore size distribution indicates that a higher n_{HCl}/n_S ratio favors the synthesis of well ordered cubic SBA-1 materials.

(46) Luzzati, V.; Vargas, R.; Mariani, P.; Gulik, A.; Delacroix, H. *J. Mol. Biol.* **1993**, *229*, 540.

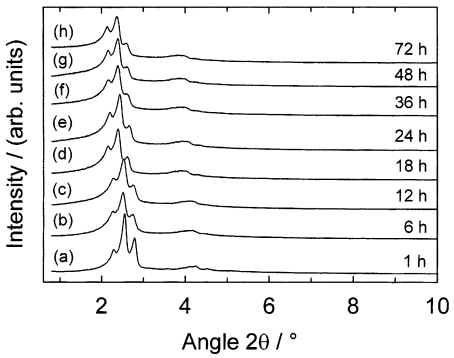

Figure 3. XRD powder patterns of SBA-1 materials prepared at different synthesis times: (a) SBA-1C; (b) SBA-1-(6H); (c) SBA-1-(12H); (d) SBA-1-(18H); (e) SBA-1-(24H); (f) SBA-1-(36H); (g) SBA-1-(48H); (h) SBA-1-(72H).

Table 2. Textural Parameters of SBA-1 Samples Prepared at Different Synthesis Times

sample	a_0 (nm)	A_{BET} (m^2/g)	pore vol (cm^3/g)	pore diam $d_{p,des}$[a] (nm)	pore diam $d_{p,ads}$[a] (nm)	pore diam $d_{p,NLDFT}$ (nm)	cage diam[b] (nm)
SBA-1C	77.7	1427	0.71	2.3	2.3	2.9	4.1
SBA-1-(6H)	79.0	1347	0.81	2.5	2.5	3.1	4.2
SBA-1-(12H)	79.5	1295	0.86	2.6	2.6	3.2	4.3
SBA-1-(18H)	82.0	1240	0.93	2.7	2.8	3.5	4.5
SBA-1-(24H)	82.0	1240	0.96	2.8	2.8	3.5	4.5
SBA-1-(36H)	82.8	1197	1.02	2.9	2.9	3.6	4.5
SBA-1-(48H)	83.1	1133	1.03	3.0	3.0	3.7	4.6
SBA-1-(72H)	83.7	1097	1.03	3.0	3.0	3.7	4.6

[a] Calculated from eq 1. [b] Calculated from eq 2.

The transition of the mesophase from disordered cubic to long-range-ordered cubic with increasing n_{HCl}/n_S ratio can be explained by the surfactant−silica assembly mechanism proposed by Huo et al.[3] According to this mechanism, the formation of the silica−surfactant mesophase under strongly acidic conditions occurs through the formation of $S^+X^-I^+$ micelles. (S^+ denotes surfactant cation, X^- the halogen anion, and I^+ the protonated inorganic SiO_2 species.) Since the I^+ species is positively charged by proton abstraction at low pH, the interaction of the surfactant S^+ with the I^+ species occurs via a $SiO_2/H^+/X^-/CTEA^+$ bridge, where the protonated silica surface is linked to the cationic surfactant headgroup via a halogen anion. With decreasing n_{HCl}/n_S ratio, the charge on the silica is reduced and the strength of the interaction between the surfactant and the inorganic species I^+ will decrease. Hence, the system will be more able to move to a more random structure. The higher concentration of protons in the gels with a higher n_{HCl}/n_S ratio will increase the charge on the silica and maintain a strong interaction with the surfactant. This situation favors a high degree of ordering, as observed in our experiments.

Variation of the Synthesis Time. Powder XRD patterns and textural properties of the calcined SBA-1 samples prepared at different synthesis times are shown in Figure 3 and Table 2, respectively. All samples exhibit a XRD pattern showing three well-resolved reflections at $2\theta = 2-3.5°$ and some higher order reflections. With increasing synthesis time, the XRD reflections are shifted to lower 2θ values, reflecting an expansion of the unit cell size (Table 2). With increasing crystallization time, the relative intensity of the (200),

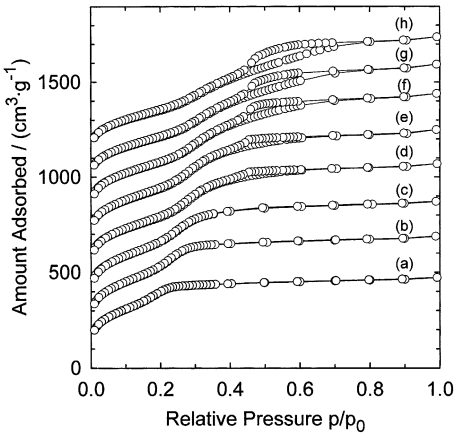

Figure 4. Nitrogen adsorption isotherms of SBA-1 materials prepared at different synthesis times: (a) SBA-1C; (b) SBA-1-(6H); (c) SBA-1-(12H); (d) SBA-1-(18H); (e) SBA-1-(24H); (f) SBA-1-(36H); (g) SBA-1-(48H); (h) SBA-1-(72H).

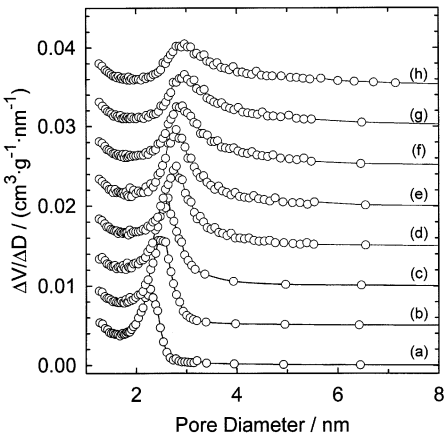

Figure 5. Pore size distribution (calculated from the adsorption branch using eq 1) of SBA-1 materials prepared at different synthesis times: (a) SBA-1C; (b) SBA-1-(6H); (c) SBA-1-(12H); (d) SBA-1-(18H); (e) SBA-1-(24H); (f) SBA-1-(36H); (g) SBA-1-(48H); (h) SBA-1-(72H).

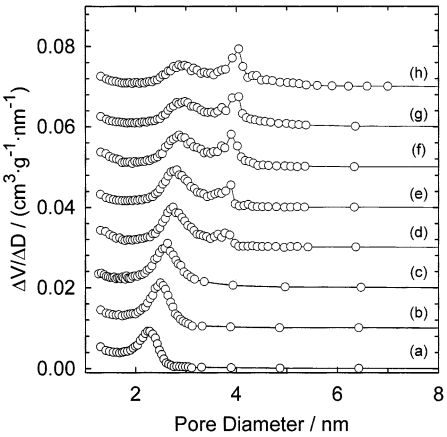

Figure 6. Pore size distribution (calculated from the desorption branch using eq 2) of SBA-1 materials prepared at different synthesis times: (a) SBA-1C; (b) SBA-1-(6H); (c) SBA-1-(12H); (d) SBA-1-(18H); (e) SBA-1-(24H); (f) SBA-1-(36H); (g) SBA-1-(48H); (h) SBA-1-(72H).

(210), and (211) reflections shifts considerably; the intensity of the (200) reflection increases, whereas the intensity of the (211) reflection is reduced. Moreover, the observed diffraction peaks can no longer be indexed in the space group $Pm\bar{3}n$, but most likely belong to a another space group with lower symmetry. It is interesting to note that the increase in unit cell size is not accompanied by a loss of structural order. It is surmised that the degree of silanol group condensation is increasing with synthesis time, yielding materials with enhanced stability.

The nitrogen adsorption isotherms of the samples prepared at different synthesis times are shown in Figure 4. The position of the capillary condensation step shifts to higher relative pressures with increasing synthesis time. Moreover, the pore volume increases from 0.7 cm^3/g for SBA-1C to 1.03 cm^3/g for SBA-1-(72H) with a concomitant decrease of the surface area from 1450 to 1100 m^2/g. Whereas the adsorption isotherm of the parent material is of type 1V according to the IUPAC classification with no hysteresis, the isotherms of the materials prepared at synthesis times longer than 24 h exhibit a H2-type hysteresis loop. With increasing synthesis time, the capillary condensation step broadens and the size of the hysteresis loop is also enlarged. The observed broad H2 hysteresis loops most likely arise from lack of uniformity of pore diameter of the materials. The shape of the adsorption−desorption isotherm has been attributed to the fact that the junctions between the cages are much narrower than the cages themselves, which causes connectivity upon nitrogen desorption. The nitrogen condensed in the cages cannot desorb until the desorption pressure for the pore mouth is reached.[47,48] Maddox et al.[49] have shown recently by means of computer simulations that pore-blocking effects in slitlike pores with narrow mouths result in adsorption isotherms that appeared to be very similar to those observed in the present study. Intrapore connectivity effects may also be an additional cause of the observed broadening of the hysteresis loop. It was also suggested that holes in broken walls of the materials act as micropores with respect to nitrogen molecules.[50] Although there is some evidence for the presence of micropores in our samples (cf. discussion on the adsorption of organics), we feel that the broadening of the hysteresis loop is most probably solely due to single-pore effects caused by the considerable variation of the pore diameter due to the cagelike structure of the SBA-1 material.

The pore size distributions calculated from the adsorption and desorption branch, respectively, of the nitrogen adsorption isotherm using the recently reported modified version of the Kelvin equation (eq 2) are shown in Figures 5 and 6. The pore size distribution calculated from the adsorption branch is uniform, but broadens significantly with increasing synthesis times. In contrast, the pore size distribution calculated from the desorption branch shows a bimodal pore size distribution from a synthesis time of 18 h onward. With synthesis time, the pore diameter increases from 2.3 to

(47) Liu, H.; Zhang, L.; Seaton, N. A. *J. Colloid Interface Sci.* **1993**, *156*, 285.
(48) Ball, P. C.; Evans, R. *Langmuir* **1989**, *5*, 714.
(49) Maddox, M. W.; Lastoskie, C. M.; Quirke, N.; Gubbins, K. E. In *Fundamentals in Adsorption*; Levan, M. D., Ed.; Kluwer: Boston, 1996; pp 571−578.
(50) Sayari, A.; Liu, P.; Kruk, M.; Jaroniec, M. *Chem. Mater.* **1997**, *9*, 2499.

3.0 nm (Table 2). A second maximum of the pore size distribution centers at 3.8 nm, which probably does not represent real pores. This maximum of the pore size distribution is typically ascribed to the so-called "tensile strength effect", which provides evidence for delayed capillary evaporation probably due to pore blocking and/or network effects. The tensile strength effect or more generalized the "instability argument" has been explained by the fact that there is a mechanical limit of the stability of meniscus of the liquid as well as a pressure ($p/p_0 = 0.42$ for N_2 at 77 K) below which the meniscus cannot hold and the pore will empty spontaneously. The minimum pressure at which a meniscus can exist is proposed to be based on the tensile strength of a fluid. The pore diameter calculated by using the nonlocal density functional theory (NLDFT) is constantly ca. 0.6 nm larger than the diameter calculated using the modified BJH equation (Table 2), whereas the width of the pore size distribution is similar in both cases.

Moreover, we used eq 2 for calculating the cage diameter of SBA-1.[45] The cage diameter increases from 4.0 to 4.6 nm with increasing synthesis time from 1 to 72 h. A possible mechanism for the observed increase in pore and cage size is that during the longer crystallization time the silica mesophase is partially dissolved and/or surfactant molecules are dissolved or displaced, inducing backflow, which will increase the density of surfactant (micellar) phase, which translates into a larger pore size as observed for the samples prepared at longer synthesis times. It is well-accepted that the synthesis of SBA-1 proceeds through the formation of triple-layered micelles, where the interaction among S^+, X^-, and I^+ is very weak in the present acidic media synthesis as compared to synthesis in a basic medium. It is noteworthy that partial dissolution of surfactant molecules or silica mesophases is preferred for the acid synthesis route because of the weaker interaction between S^+, X^-, and I^+.

Under basic conditions at elevated temperature, Hoffmann degradation to form neutral amines from quaternary ammonium salts is fairly facile, and as a result, it has been implicated in pore swelling upon hydrothermal treatment in alkaline conditions.[51] It is, however, unlikely that this reaction plays a significant role in pore swelling under acidic conditions.

It also has to be considered that the charge density of the silica polymorphs is decreased by a higher degree of condensation as a result of the prolonged crystallization time, which could result in the detachment of surfactant cations from the negatively charged silica framework. The released surfactant cations could also act as a swelling agent, resulting in an increased pore diameter of SBA-1. However, the complete mechanism of tuning the pore diameter of SBA-1 and the possible phase transformation are still not fully understood. Further studies are needed to clarify the formation mechanism.

TGA measurements have been undertaken to characterize the SBA-1 samples prepared in this study. The DTG curve (Figure 7) of the as-synthesized parent SBA-1 shows five distinct maxima at 55, 240, 283, 340, and >500 °C. The first weight loss (ca. 1.9 wt %) is ascribed to desorption of water molecules physisorbed on the external surface area of the crystallites or occluded in the macropores and mesopores located between the crystallites. The second (ca. 26 wt %) and third (ca. 3.2 wt %) weight losses occur at 240 and 283 °C, respectively, and are attributed to the desorption and/or decomposition of the template forming hexadecene and triethylamine via an Hoffmann-type degradation ($C_{16}H_{33}N(C_2H_5)_3^+ \rightarrow C_{16}H_{32} + N(C_2H_5)_3 + H^+$). The fourth weight loss (10.4 wt %) at ca. 340 °C is assigned to the combustion of the remaining template molecules or template fragments (e.g., adsorbed trimethylamine or alkenes); the last broad peak around 530 °C, which is due to the dehydroxylation of SiOH groups,[52] amounts to a weight loss of about 8.6 wt %. The DTG curves of the samples prepared at higher synthesis times exhibit four distinct maxima at 60, 255, 328, and 540 °C (Figure 7). A weight loss at ca. 283 °C as observed for the parent SBA-1C is not observed for the SBA-1 samples synthesized at longer synthesis time. The diffusion of the template molecules or template fragments is most likely facilitated by the increased pore diameter, which results in a coalescence of the two maxima at 240 and 283 °C to a single maximum around 255 °C.

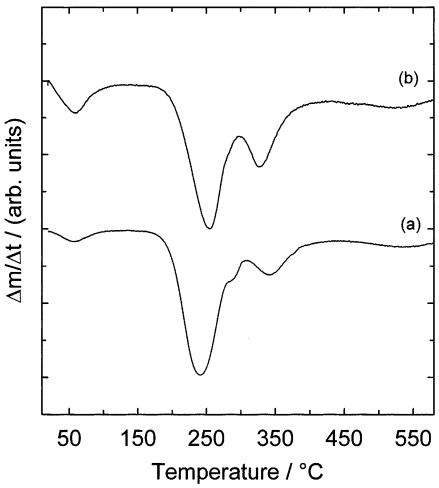

Figure 7. DTG curves of as-synthesized SBA-1 materials synthesized at different synthesis times: (a) SBA-1C and (b) SBA-1-(72H).

Stability of SBA-1 after Washing with Water. It has been observed that SBA-1 is not stable after synthesis toward washing with water, which results in structural degradation. The low stability of SBA-1 in water is a result of the low degree of cross-linking of the silica walls, which are prone to hydrolysis, resulting in partial structural collapse. To probe the stability of SBA-1 in the presence of water, we have tested different SBA-1 samples, which were synthesized between 1 and 72. Figure 8 exhibits the XRD patterns of calcined SBA-1-(*n*H) samples after washing with water, which were kept at 100 °C for 1, 24, 48, and 72 h, respectively. The stability toward water increases with synthesis time. The N_2 adsorption−desorption isotherms of the washed samples are shown in Figure 9. Comparison between

(51) Cheng, C.-F.; Zhou, W.; Park, D. H.; Klinowski, J.; Hargreaves, M.; Gladden, L. F. *J. Chem. Soc., Faraday Trans.* **1997**, *93*, 359.

(52) Basu, P.; Ballinger, T. H.; Yates, J. T., Jr. *Rev. Sci. Instrum.* **1988**, *59*, 1321.

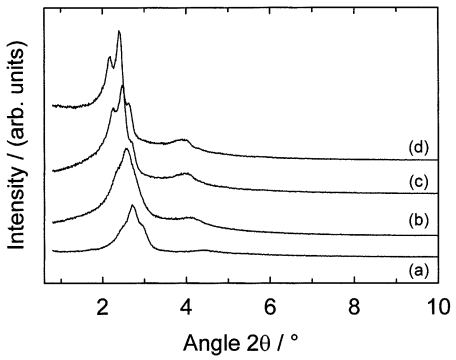

Figure 8. XRD powder patterns of SBA-1 materials prepared at different synthesis times after washing with water: (a) SBA-1-(1HW); (b) SBA-1-(24HW); (c) SBA-1-(48HW); (d) SBA-1-(72HW).

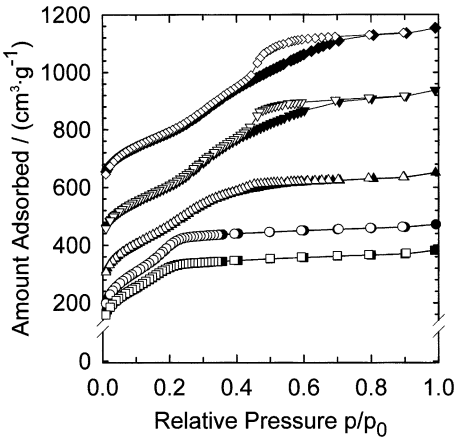

Figure 9. Nitrogen adsorption isotherms (adsorption, closed symbols; desorption, open symbols) of SBA-1 materials prepared at different synthesis times after washing with water: (●) SBA-1-(1HW); (■) SBA-1 (1H); (▲) SBA-1-(24HW); (▼) SBA-1-(48HW); (◇) SBA-1-(72HW).

Table 3. Textural Parameters of SBA-1 Prepared at Different Synthesis Times after Washing with Water

sample	synthesis time (h)	a_0 (nm)	A_{BET} (m^2/g)	pore vol (cm^3/g)	pore diam $d_{p,des}$[a] (nm)	pore diam $d_{p,ads}$[a] (nm)
SBA-1-(1HW)	1	72.6	1099	0.57	2.2	2.2
SBA-1-(24HW)	24	76.7	1123	0.74	2.6	2.6
SBA-1-(48HW)	48	80.1	1099	0.94	2.9	2.9
SBA-1-(72HW)	72	82.4	1097	0.97	2.9	2.9

[a] Calculated from eq 1.

Figures 9 and 4 shows that there is a significant difference in the amount of nitrogen adsorbed and the height of the capillary condensation step before and after washing with water for the parent material SBA-1. But the sample synthesized longer than 24 h showed almost the same isotherm after washing as compared to the unwashed parent material. This indicates that prolonged synthesis time results in samples with increased stability toward hydrolysis. Textural properties of these samples after washing with water are summarized in Table 3. It can be seen that specific surface area and pore volume are drastically reduced after washing with water prior to calcination due to partial structural collapse of SBA-1-(1HW) and SBA-1-(24HW). However, SBA-1-(48HW) and SBA-1-(72HW) do not show an appreciable degradation after exposure to water. Surface area, pore volume, and pore diameter of the later materials, viz., SBA-1-(48H) and SBA-1-(72H), are only slightly reduced as compared to those of the parent materials, which were prepared under the same conditions, but not subjected to water washing. We assume that the lower degree of cross-linking of the silica species is responsible for the lower stability of the SBA-1 samples prepared at shorter synthesis times. A synthesis time of 48 h is needed to induce sufficient cross-linking to prevent structural collapse via hydrolysis of siloxane bonds.

Table 4. Textural Parameters of the Pressed SBA-1 Materials

sample	pelletizing pressure (MPa)	a_0 (nm)	A_{BET} (m^2/g)	pore vol (cm^3/g)	pore diam $d_{p,ads}$[a] (nm)
SBA-1(0)	0	77.7	1427	0.71	2.3
SBA-1(43)	43	78.0	1297	0.69	2.4
SBA-1(107)	107	77.4	1151	0.60	2.3
SBA-1(217)	217	76.5	1105	0.57	2.3

[a] Calculated from eq 1.

Mechanical Stability. The powder XRD patterns and the nitrogen adsorption isotherms of the compressed SBA-1 samples are found in the Supporting Information. The intensity of the reflections decreases only slightly with pelletizing pressure, up to a pressure of 217 MPa. A significant decrease of reflection intensity accompanied by an increased line broadening is observed after pressing the material with 217 MPa. The (200), (210), and (211) reflections and the higher order reflections do not shift considerably with pressure, which indicates only minor changes of the SBA-1 unit cell. With increasing pelletizing pressure, the amount of adsorbed nitrogen decreases. However, in comparison to other mesoporous materials, viz., MCM-41, MCM-48, and SBA-15,[33−43] the decrease in adsorption capacity is small. Furthermore, with increasing pelletizing pressure, specific pore volume and surface area decrease moderately (Table 4). The pore size distribution broadens slightly with increasing pelletizing pressure (Supporting Information). A similar trend was also observed in earlier studies on MCM-48.[33]

To evaluate the accessibility of the SBA-1 pore system after compression to larger probe molecules with relevance to catalysis, the adsorption of organics such as cyclohexane and *n*-heptane has been investigated. The adsorption isotherms of cyclohexane and *n*-heptane at 298 K for the pressed SBA-1 materials in comparison to the parent material SBA-1C are shown in Figures 10 and 11, respectively. All adsorption isotherms are of type IV according to the IUPAC classification. The total uptake of organics after the pore condensation is complete is used to calculate the total pore volume (by applying the Gurvich rule) accessible to larger molecules such as *n*-heptane and cyclohexane. Pore volumes were calculated from the amount adsorbed, assuming that the density of the adsorbed phase is equal to the density of bulk liquid at adsorption temperature. The pore volumes calculated from the *n*-heptane and cyclohexane adsorption isotherms obtained at different temperatures are summarized in Table 5. The pore volumes calculated from the uptake of *n*-heptane and cyclohexane are significantly lower compared to the pore volumes de-

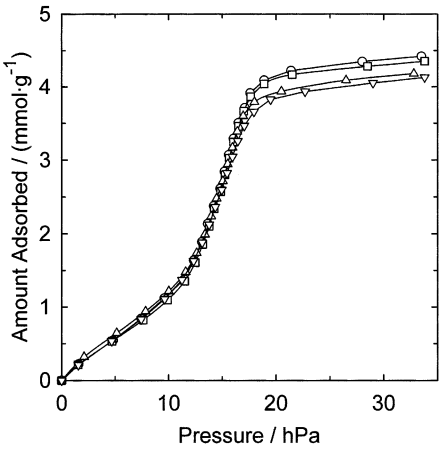

Figure 10. Cyclohexane adsorption isotherms for the pressed SBA-1 materials: (○) SBA-1(0); (□) SBA-1(43); (△) SBA-1(107); (▽) SBA-1-(217).

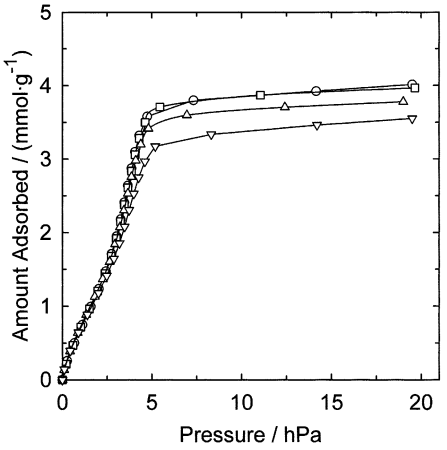

Figure 11. *n*-Heptane adsorption isotherms for the pressed SBA-1 materials: (○) SBA-1(0); (□) SBA-1(43); (△) SBA-1(107); (▽) SBA-1-(217).

termined from nitrogen adsorption (Figure 12). In previous studies on MCM-41 and MCM-48, it was also found that the pore volumes determined by adsorption of subcritical organic vapors are systematically lower (10−20%) than the ones calculated from nitrogen data.[33,53] This was mainly ascribed to the uncertainty of the density of the adsorbed phase, which is taken as the density of bulk liquid at the adsorption temperature (Gurvich rule). Recently, Ribeiro Carrot et al. showed that the density of the nitrogen in the pores is higher than the normal bulk liquid density.[53] With a change in the normal bulk density of nitrogen from 0.808 to 0.84 g cm^{-3}, almost the same pore volume is obtained from organic and nitrogen adsorption on MCM-41. For SBA-15, a large discrepancy (up to 50%) was observed between the pore volume determined by nitrogen adsorption and organics adsorption.[34,35] This discrepancy was ascribed to a significant amount of micropores, which are not accessible to large organics such as benzene or *n*-heptane. We, therefore, tentatively assume that the presence of micropores has to be considered for SBA-1 as well. It is at present not clear whether the observed microporosity is a structural feature of SBA-1

(53) Ribeiro Carrott, M. M. L.; Candeias, A. J. E.; Carrott, P. J. M.; Ravikovitch, P. I.; Neimark, A. V.; Sequeira, A. D. *Microporous Mesoporous Mater.* **2001**, *47*, 323.

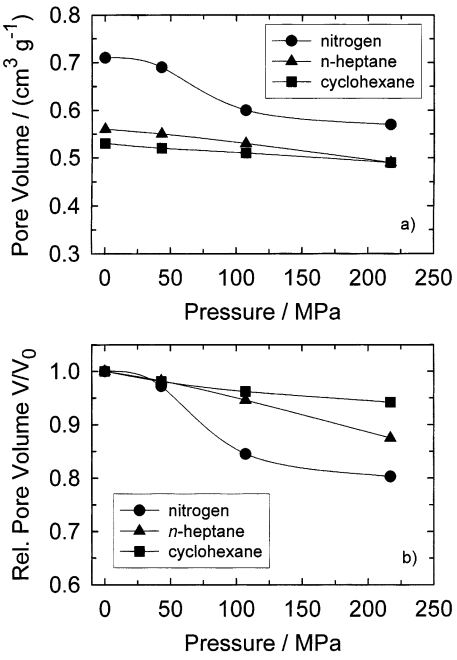

Figure 12. Comparison of (a) pore volume and (b) relative pore volume V/V_0 of SBA-1 determined by nitrogen (●), *n*-heptane (▲), and cyclohexane (■) adsorption.

or is due to structural defects in the amorphous walls. Upon compression at 217 MPa, the pore volume calculated from nitrogen adsorption decreases by 19.7%, whereas the pore volume calculated from *n*-heptane and cyclohexane adsorption declines by 12.5% and 7.5%, respectively. These results indicate that the structure of SBA-1 has comparable stability to the cubic MCM-48 phase,[33] but exhibits higher stability as compared to the structures of MCM-41 and SBA-15.[34,35]

It is interesting to note that the discrepancy between the pore volumes calculated from nitrogen and organics adsorption decreases with increasing pelletizing pressure. The molecular diameters of the adsorbates increases in the order nitrogen < *n*-heptane < cyclohexane. The pore volumes calculated from the cyclohexane adsorption decreases linearly from 0.53 to 0.49 cm^3 g^{-1}, whereas the pore volume calculated from the nitrogen adsorption isotherm decreases from 0.71 to 0.57 cm^3 g^{-1} (Figure 12a). From the discrepancy between the pore volumes calculated from nitrogen and organics adsorption it was already concluded that the SBA-1 samples prepared in the present study contain micropores. The decrease of pore volume observed by nitrogen adsorption suggests that the micropore volume decreases to a larger extent as compared to the mesopore volume. A possible explanation for this finding is that the micropores are blocked upon compression and are no longer accessible for nitrogen. Furthermore, in the case that the microporosity is due to structural defects in the amorphous walls, one could assume that the particles with a higher content of structural defects are mechanically less stable and are preferentially destroyed upon compression.

The relative pore volume V/V_0 (V_0 is the pore volume of the unpressed parent material) calculated from both nitrogen and organics adsorption for unpressed and pressed materials is a good measure for the mechanical stability of porous materials (Figure Figure 12b). The decline in relative pore volume is smaller for SBA-1 as

Table 5. Adsorption of *n*-Heptane and Cyclohexane (CHx) of SBA-1 Materials Pressed at Different Pelletizing Pressures

	V_p (N_2) ($cm^3\ g^{-1}$)	n_{ads}(*n*-heptane) (mmol g^{-1})			V_p (*n*-heptane) ($cm^3\ g^{-1}$)			n_{ads} (CHx) (mmol g^{-1})	V_{cal} (CHx) ($cm^3\ g^{-1}$)
temperature (K):	77	283	298	313	283	298	313	298	298
SBA-1(0)	0.71	3.89	3.80	3.73	0.56	0.56	0.56	4.09	0.53
SBA-1(43)	0.69	3.77	3.70	3.69	0.55	0.55	0.55	4.04	0.52
SBA-1(107)	0.60		3.59			0.53		3.94	0.51
SBA-1(217)	0.57		3.33			0.49		3.83	0.49

compared to that of hexagonal phases such as MCM-41 and SBA-15, but similar as compared to that of MCM-48.[33] This confirms that a cubic arrangement of pores can withstand a higher compression strain than a hexagonal pore arrangement of similar pore diameter and wall thickness. In agreement with previous studies on MCM-48 and MCM-41,[33,40,43] the loss in pore volume is accompanied only by a minor decrease in pore size, which confirms that the decrease in specific pore volume and surface area is a consequence of subsequent crushing of primary particles upon compression. Similar conclusions have also been drawn for other mesoporous materials.[25,40,43]

Conclusions

The cubic mesoporous phase SBA-1 has been synthesized under different conditions and characterized by X-ray powder diffraction (XRD), nitrogen adsorption, and thermogravimetric analysis (TGA). The current study shows that the structural order of SBA-1 can be improved by increasing the n_{HCl}/n_S ratio. It also has been discovered that the pore diameter of SBA-1 can be controlled by simply adjusting the crystallization time. The pore diameter can be increased from 2.2 to 3 nm by raising the synthesis time from 1 to 72 h without a significant decrease in structural order. However, a phase transformation resulting in a change of the space group from $Pm\bar{3}n$ to a space group with lower symmetry cannot be ruled out. The materials prepared at extended synthesis time have also shown improved stability toward washing with water. The observed increase in stability is probably due to an enhanced cross-linking of silica species, which hinders hydrolysis of siloxane bonds as observed for samples prepared at reduced synthesis time. The mechanical stability of SBA-1 has been studied by XRD, nitrogen as well as *n*-heptane and cyclohexane adsorption. Upon compression at 217 MPa, the pore volume as determined by nitrogen adsorption decreases by 19.7%, whereas the pore volume calculated from the *n*-heptane and cyclohexane adsorption declines by 12.5% and 7.5%, respectively. These results indicate that the presence of microporosity in the SBA-1 pore walls has to be considered. It follows from the present study that SBA-1 is mechanically more stable as compared to MCM-41 and SBA-15, whereas its stability is comparable to the stability of MCM-48. The observed reduction of the pore volume is probably due to a partial destruction of the SBA-1 pore system, whereas the rest of the material is completely unaffected by the compression.

Acknowledgment. Financial support of this work by Deutsche Forschungsgemeinschaft (Ha2527/4-1) and Fonds der Chemischen Industrie is gratefully acknowledged. M.H. thanks Professor S. Ernst for generous support.

Supporting Information Available: Figures with the Powder X-ray diffraction patterns, nitrogen adsorption isotherms, and pore size distributions of compressed SBA-1 (PDF). This material is available free of charge via the Internet at http://pubs.acs.org.

CM0213523